Noname manuscript No.
(will be inserted by the editor)

Effects of rotation and mid-troposphere moisture on organized convection and convectively coupled waves

Andrew J. Majda · Boualem Khouider · Yevgeniy Frenkel

Received: date / Accepted: date

Abstract Atmospheric convection has the striking capability to organize itself into a hierarchy of cloud clusters and super-clusters on scales ranging from the convective cell of a few kilometres to planetary scale disturbances such as the Madden-Julian oscillation. It is widely accepted that this phenomenon

Andrew J. Majda
Department of Mathematics, Center for Atmosphere-Ocean Science, Courant Institute, and Center for Prototype Climate Modeling, NYU Abu Dhabi Institute
New York University
251 Mercer Street
New York, NY 10012 USA
Tel.: 212-998-3234
Fax: 212-995-3323
E-mail: jonjon@cims.nyu.edu

Boualem Khouider
Department of Mathematics and Statistics
University of Victoria
PO BOX 3045 STN CSC
Victoria, BC
Canada V8W 3P4
Tel. 250-721-7439
Fax. 250-721-8962
E-mail: khouider@math.uvic.ca

Yevgeniy Frenkel
Department of Mathematics and Center for Atmosphere-Ocean Science, Courant Institute
New York University
251 Mercer Street
New York, NY 10012 USA
Tel.: 212-998-3234
Fax: 212-995-4121
E-mail: frenkel@cims.nyu.edu

is due in large part to the two-way coupling between convective processes and equatorially trapped waves and planetary scale flows in general. However, the physical mechanisms responsible for this multiscale organization and the associated across-scale interactions are poorly understood. The two main peculiarities of the tropics are the vanishing of the Coriolis force at the equator and the abundance of mid-level moisture. Here we test the effect of these two physical properties on the organization of convection and its interaction with gravity waves in a simplified primitive equation model for flows parallel to the equator. Convection is represented by deterministic as well as stochastic multicloud models that are known to represent organized convection and convectively coupled waves quite well. It is found here that both planetary rotation and mid-troposphere moisture are important players in the diminishing of organized convection and convectively coupled wave activity in the subtropics and mid-latitudes. The meridional mean circulation increases with latitude while the mean zonal circulation is much shallower and is dominated by mid-level jets, reminiscent of a second baroclinic mode circulation associated with a congestus mode instability in the model. This is consistent with the observed shallow Hadley and Walker circulations accompanied by congestus cloud decks in the higher latitude tropics and sub-tropics associated with the monsoon trough and with the northward migration of the intra-tropical convergence zone. Moreover, deep convection activity in the stochastic model simulations becomes very patchy and unorganized as the computational domain is pushed towards the subtropics and mid-latitudes. This is consistent with previous work based on cloud resolving modeling simulations on smaller domains.

Keywords Rotation effects · Congestus clouds · Convectively coupled waves · Organized convection · Stochastic parametrization · Tropical circulation

1 Introduction

Atmospheric dynamics in the tropics are characterized by the predominance of organized deep convection on a wide range of scales, spanning mesoscale systems to synoptic and planetary scale convectively coupled waves such as Kelvin waves and the Madden Julian oscillation (MJO) [21,33,19]. A few key physical processes are believed to play a central role in defining these characteristic features of tropical dynamics: the vanishing of the Coriolis force at the equator, the abundance of moisture over of the warm waters of the tropical oceans and rain forests, and the ability of convection and in particular clouds to transport and redistribute this moisture in the vertical. The goal here is elucidate the effects of rotation and of the mean vertical moisture profile on organized convection on the planetary scale and on the induced mean circulation, using simple multicloud models for convectively coupled waves.

The setup consists of the multicloud model of Khouider and Majda [15,18] in 2 dimensions (x, z) on an f-plane where the Coriolis parameter f varies from $f = 0$, at the equator, to larger values for higher latitudes. As demonstrated in earlier papers, the multicloud model is very good at simulating convectively coupled waves, including the MJO, from both the stand point of linear theory [15,26,18,17] and in idealized climate simulations [16,26,18,20]. In the 2D setup in particular, where the beta effect is ignored, convectively coupled waves are allowed to travel in both east-west directions as gravity waves, see [15,26,16,18] for flows above the equator ($f = 0$).

Here we show through simple simulations and linear theory that the introduction of rotation effect in the 2d multicloud model induces (1) a non-zero meridional circulation which increases with f, reminiscent of the Hadley circulation and (2) a decrease in the zonal circulation due to less moisture coupling as the simulated flow transit from a deep mean circulation driven by deep and stratiform convection to a shallow circulation driven by congestus cloud decks. Moreover, as the parameter f is increased (1) the strength of the moisture fluctuations decreases rapidly and (2) the wave fluctuations lose their coherence as packets of convectively coupled waves while precipitation and deep convection become increasingly patchy and localized. This last fact is consistent with earlier work by Liu and Moncrieff [22], using cloud resolving modeling on smaller domains (more on this below).

The results of such studies, in a simplified setting, can be used to understand the transition of convectively coupled synoptic systems from the tropics to sub-tropics such as the behavior of convectively coupled waves in the ITCZ [8, 9, 7, 23] and in monsoon troughs with respect to changes in the effects of rotation and environmental moisture as these systems move poleward [6, 5, 32, 28].

The effect of rotation on gravity waves and convection is studied in Liu and Moncrieff [22] using a two dimensional (x, z) non-hydrostatic primitive equations model with rotation effects. They first looked at the steady state mesoscale response to a localized convective scale heat source with various vertical profiles to mimic variability in proportions of deep and stratiform heating. They found that the main effect of rotation on convection is that the induced subsidence becomes more and more confined to the vicinity of the heating source. The authors concluded that, in a moist atmosphere, such confinement by rotation would stabilize and dry the environment near mature convective peaks and thus would inhibit the formation of cloud clusters on the meso- and synoptic scales. They then conducted cloud resolving modeling simulations using the same set up to test their hypothesis on a 4000 km domain. Among three different settings, tropics, sub-tropics, and midlatitudes, they found that convective clustering is observed only in the tropics, when $f = 0$, where, under the influence of an easterly mean flow, convection further organizes into westward propagating moist gravity waves. The main effect of planetary rotation is that convection becomes patchy and unorganized regardless of the presence or not of a mean-flow. The effect of convective precipitation on geostrophic adjustment for the f-plane, is studied in Dias and Pauluis [1] using a simple one-baroclinic quasi-equilibrium model [4]. They found that convective precipitation induces a delay in the adjustment process and leads to both a stronger temperature gradient and stronger jets. This is an indication that convection has a certain effect on dry dynamics in midlatitudes but not as much as it does in the tropics.

The rest of the paper is organized as follows. The multicloud model on an f-plane is presented in Section 2 and the effect of rotation on its linear waves and instabilities is studied in Section 3. Nonlinear simulations using both the deterministic and stochastic multicloud models [13, 2, 3] with rotation are presented in Section 4. In particular, the stochastic simulations reproduce qualitatively the behavior seen in the CRM results of Liu and Moncrieff [22] especially regarding the patchiness of deep convection as the Coriolis effect increases. This is significant since it is already demonstrated in earlier work [2, 3, 30] that the stochastic multicloud model mimics quite well the chaotic behavior and the stochastic organization of deep convection. Section 5 concludes the paper with a summary and discussion.

2 The model and setup

As pointed out in the introduction we use the multicloud model of Khouider and Majda in the simple setup of 2d flows parallel to the equator [18]. This choice is made because this is a simple model of intermediate complexity on which linear analysis can be easily performed (with a linear algebra software such as Matlab) and yet it is a good model for convectively coupled equatorial waves [15,18,17, etc.] and organized convective systems in general [20,26,10, 14]. To better represent the chaotic behavior of organized convection we also use the stochastic version of the multicloud model first introduced in Khouider et al. [13]. The stochastic multicloud model captures well the chaotic behavior of organized convection as seen in CRMs [2,3] and the stochastic variability of convective precipitation in radar observations [30].

The dynamical core equations of the multicloud model in a two dimensional setting, parallel to the equator, can be summarized as follows. The main model is based on the hydrostatic primitive equations, with a coarse vertical resolution reduced to the first two baroclinic modes, where the advection nonlinearities are ignored. The background climatology consists of a homogeneous stratification with a constant Brunt-Väisälä buoyancy frequency and a moisture profile exponentially decaying in the vertical [15]. More details on the derivation of the model equations are found in the seminal papers [15, 18]. The perturbation fluid dynamic variables assume the following reduced expansions in the vertical.

$$\begin{aligned} U(x,z,t) &= u_1(x,t)\sqrt{2}\cos(z) + u_2(x,t)\sqrt{2}\cos(2z) \\ V(x,z,t) &= v_1(x,t)\sqrt{2}\cos(z) + v_2(x,t)\sqrt{2}\cos(2z) \\ \Theta(x,z,t) &= \theta_1(x,t)\sqrt{2}\sin(z) + 2\theta_2\sqrt{2}\sin(2z), \end{aligned} \tag{1}$$

where U, V are respectively the zonal and meridional velocity components and Θ is the potential temperature. The indexed variables $(.)_1$ and $(.)_2$ are the corresponding first and second baroclinic components. Here x is the zonal coordinate (longitude) and z is the vertical coordinate (altitude), $0 \leq x \leq P_y,\ 0 \leq z \leq \pi$ where P_y is Earth's perimeter at latitude y and z varies in units of the tropospheric height $H_T \approx 16$ km. The vertical velocity and pressure fields are obtained through the continuity and hydrostatic balance equations, respectively. The equations of motion for the first and second baroclinic modes, augmented by the vertically averaged tropospheric moisture perturbation, q, and the boundary layer equivalent potential temperature θ_{eb}, are given by

$$
\begin{aligned}
&\frac{\partial u_j}{\partial t} - f v_j - \frac{\partial \theta_j}{\partial x} = -d u_j \\
&\frac{\partial v_j}{\partial t} + f u_j = -d v_j, j = 1, 2 \\
&\frac{\partial \theta_1}{\partial t} - \frac{\partial u_1}{\partial x} = H_d + \xi_s H_s + \xi_c H_c - S_1 \\
&\frac{\partial \theta_2}{\partial t} - \frac{1}{4}\frac{\partial u_2}{\partial x} = -H_s + H_c - S_2 \\
&\frac{\partial q}{\partial t} + \frac{\partial}{\partial x}(u_1 q + \alpha u_2 q) + \tilde{Q}(u_1 + \tilde{\lambda})\frac{\partial q}{\partial x} = -P + \frac{1}{H} D \\
&\frac{\partial \theta_{eb}}{\partial t} = -\frac{1}{h} D + \frac{1}{h} E.
\end{aligned}
\tag{2}
$$

Here $f = 2\Omega \sin(\phi_y)$ is the Coriolis parameter at the fixed latitude with ϕ_y the corresponding angle and $\Omega = 2\pi/24$ hours while $d = \left(C_d \frac{u_0}{h} + \frac{1}{\tau_R}\right)$ is the sum of boundary layer and Rayleigh friction coefficients. Here H_d, H_s, H_c are the deep, stratiform and congestus heating rates while $P = H_d + \xi_s H_s + \xi_c H_c$ is the moisture sink due to precipitation reaching the ground and D represents downdrafts that tend to moisten the environment due to evaporation of deep convective and stratiform rain and cool and dry the boundary layer. The effect of radiative cooling is represented by the terms S_1, S_2 while E represents the evaporation from the sea surface. Further details about the multicloud model equations, in particular regarding the parametrization of H_d, H_s, H_c are provided in Table 1 for the stochastic and deterministic models, separately. The stochastic multicloud model is discussed further in Section 4.3. The interested reader is referred to the original multicloud papers for more details [15,18,13].

The equations in (2) are written in non-dimensional units where the equatorial Rossby deformation radius $Le = \sqrt{c/\beta} \approx 1500$ is the length scale, $c \approx 50$

m s^{-1}, the first baroclinic dry gravity wave speed, is the velocity scale, and $T = \sqrt{c\beta}^{-1} \approx 8.33$ hours is the time scale. The temperature scale is fixed to $\overline{\alpha} = H_T/piN^2\theta_0/g \approx 15K$ with $\theta_0 = 300$ K a reference temperature, $g = 9.8$ m s^{-2} is the gravity acceleration and $N = 0.01$ s^{-1} is the Brunt-Väisälä frequency. The drag parameter d has the same value used in previous studies using the multicloud model with $d = 4.15 \times 10^6$ s^{-1}.

As illustrated below, the two key parameters that control the geostrophic-radiative-convective or moist-geostrophic adjustment are d and f. In fact, if we denote by $\langle . \rangle$ the statistical (time-average) steady-state operator then, at statistical steady state, the system in (2) yields the equations

$$\begin{aligned}
&-f\langle v_j\rangle - \langle \theta_j\rangle_x = -d\langle u_j\rangle \\
&f\langle u_j\rangle = -d\langle v_j\rangle, j = 1,2 \\
&\langle u_1\rangle_x = \langle P - S_1\rangle \\
&\frac{1}{4}\langle u_2\rangle_x = \langle -H_s + H_c - S_2\rangle \\
&\langle P\rangle + \langle qu_1 + \tilde{\alpha} uq_2\rangle_x + \tilde{Q}\left(\langle u_1\rangle_x + \tilde{\lambda}\langle u_2\rangle_x\right) = \frac{1}{H_T}\langle D\rangle \\
&= \frac{1}{H_T}\langle E\rangle = \frac{h}{H_T}\frac{1}{\tau_e}(\theta^*_{eb} - \overline{\theta_{eb}} - \langle \theta_{eb}\rangle)
\end{aligned} \tag{3}$$

The first two equations in (3) can be rearranged to yield

$$\begin{aligned}
\langle v_j\rangle &= -\frac{f}{d}\langle u_j\rangle \\
\langle \theta_j\rangle_x &= \left(\frac{f^2}{d} + d\right)\langle u_j\rangle, j = 1,2,
\end{aligned} \tag{4}$$

which together with the 3rd and fourth equation imply that the strength of the moist-geostrophic adjustment is controlled by the balance between the strength of rotation and dissipation through the ratio f/d. Clearly, the first equation in (4) implies that the ratio of the strength of the mean meridional winds to the mean zonal winds increases with the strength of rotation. The other factors that control the strength of the mean circulation are the external forcing, i.e, the imposed radiative cooling $Q^0_{R,1}$, the evaporative flux $\frac{1}{\tau_e}(\theta^*_{eb} - \bar{\theta}_{eb})$, and the dryness of the middle troposphere $\overline{\theta}_{eb} - \overline{\theta}_{em}$. Here, the constants $\bar{\theta}_{eb}, \bar{\theta}_{em}$ are equivalent potential temperatures of a background homogeneous sounding taken as an RCE solution [26,18,17].

The third and fourth equations in (3) indicate that the statistical steady state automatically satisfies the weak temperature gradient balance, where the vertical velocity or horizontal divergence is balanced by convective heating [31,25,24]. However, we can see from (4) that, when the mean zonal flow is sufficiently strong, departures from weak temperature gradient can be important for sufficiently large f; namely if $f^2/d \gtrapprox 1$ in the non-dimensional units, i.e, $f \gtrapprox f_0 = \sqrt{d/T} \approx 1.0169$ day^{-1} which is equivalent to latitudes $\phi_y = \sin^{-1}(f_0/(2\pi\Omega)) \approx 1.5^o$ or 160 km.

It is worthwhile to recall [15,18,13] that for any solution of (2), the vertically integrated equivalent potential temperature, $\theta_e^{tot} = \frac{h}{H_T}\theta_{eb} + \theta_1 + q$, satisfies

$$\frac{\partial \theta_e^{tot}}{\partial t} = -\frac{\partial}{\partial x}\left[q(u_1 + \tilde{\alpha} u_2)\right] + (1 - \tilde{Q})\frac{\partial u_1}{\partial x} - \tilde{Q}\tilde{\lambda}\frac{\partial u_2}{\partial x} + \frac{1}{H_T}E - S_1.$$

Thus, vertically integrated moist static energy remains conserved in the absence of external forcing regardless of rotational effects.

3 Effect of Rotation and atmospheric dryness on linear stability

In this section, we report linear stability results for the system in (2) when the two key parameters identified above, namely, the Coriolis parameter f and the dryness of the middle troposphere of the background-RCE solution, $\bar{\theta}_{eb} - \bar{\theta}_{em}$, are varied. We use the same linearization procedure as in [15,18]. The inter-

Table 1 Convective closures for the deterministic and stochastic multicloud parametrization. The over-barred quantities are physical constants uniquely determined by the choice of the radiative convective equilibrium. See text for details.

Physical quantity	Deterministic	Stochastic
Potential for deep convection	$Q_d = \bar{Q} + \tau_{conv}^{-1}[a_1\theta_{eb} + a_2 q - a_0(\theta_1 + \gamma_2\theta_2)]^+$	
Potential for congestus	$Q_c = \bar{Q} + \tau_{conv}^{-1}[\theta_{eb} - a_0'(\theta_1 + \gamma_2'\theta_2)]^+$	
Convective available potential energy (CAPE)		$CAPE = \overline{CAPE} + R(\theta_{eb} - \gamma(\theta_1 + \gamma_2\theta_2))$
Low level CAPE		$CAPE_l = \overline{CAPE} + R(\theta_{eb} - \gamma(\theta_1 + \gamma_2'\theta_2))$
Midlevel θ_e	$\theta_{em} = q + \frac{\sqrt{2}}{\pi}(\theta_1 + \alpha_2\theta_2)$	
Moisture switch function	$\Lambda = 1$ if $\theta_{eb} - \theta_{eb} \geq 20$K $\Lambda = 0$ if $\theta_{eb} - \theta_{eb} \leq 10$K Linear and continuous otherwise	
Congestus heating	$\partial_t H_c = \frac{1}{\tau_c}(\alpha_c \Lambda Q_c^+ - H_c)$	$H_c = \sigma_c \frac{\alpha_c \bar{\alpha}}{H_m}\sqrt{CAPE_l^+}$,
Deep convection	$H_d = (1-\Lambda)Q_d^+$,	$H_d = [\sigma_d \bar{Q} + \frac{\sigma_d}{\bar{\sigma}_d \tau_{conv}}(a_1\theta_{eb} + a_2 q - a_0(\theta_1 + \gamma_2\theta_2))]^+$,
Stratiform heating	$\partial_t H_s = \frac{1}{\tau_s}(\alpha_s H_d - H_s)$	$\partial_t H_s = \frac{1}{\tau_s}(\alpha_s \sigma_s H_d/\bar{\sigma}_d - H_s)$

ested reader is referred to those papers for the details. As demonstrated in [18], for flows above the equator ($f = 0$), the dryness parameter, $\bar{\theta}_{eb} - \bar{\theta}_{em}$, has a major impact on the instability features of the system. In the standard parameter regime of [18] (referred to below as the KM08 parameter regime), for a moist atmosphere with $\bar{\theta}_{eb} - \bar{\theta}_{em} \approx 10$ to 12 K, the multicloud equations (2) exhibit moist gravity waves as the dominant instability, peaking at synoptic scales, with the associated modes having the physical and dynamical features reminiscent of convectively coupled Kelvin waves, including a reduced phase speed of ≈ 17 m/s and the observed front-to-rear tilt in zonal winds, temperatures, and heating anomalies. As the atmosphere becomes dryer a secondary instability of a planetary scale standing congestus mode develops and amplifies when $\bar{\theta}_{eb} - \bar{\theta}_{em} \gtrapprox 14$ K and becomes dominant while the moist gravity wave instability (MGWI) fades out. This collapse of MGWI can be viewed as the equivalent of the collapse of convectively coupled waves as one moves

Table 2 The KM08 and FMK13 parameter regimes. Parameters assuming the same value are repeated on the last column.

Parameter	Description	KM08	FMK13
a_1	Coefficient of θ_{eb} in deep convection closure	0.45	0.5
a_2	Coefficient of q in deep convection closure	0.55	0.5
a_0	Coefficient of $\theta_1 + \gamma_2\theta_2$ in deep convection closure	5	2
τ_{conv}	Convective time scale	2 hrs	-
a'_0	Inverse buoyancy scalling	1.5	-
γ'_2	Relative contribution of θ_2 in congestus heating closure	2	0.1
$\alpha_2 = 0.1$	Contribution of θ_2 to θ_{em}	0.1	-
τ_c	Congestus adjustment time scale	1 hr	-
α_c	Congestus adjustment fraction	0.1	-
τ_s	Stratifrom adjustment time scale	3 hrs	-
α_s	Stratiform adjustment fraction	0.25	-

from the moist environment of the equatorial atmosphere towards the dryer higher latitudes. The transition to a congestus standing mode instability is consistent with the abundance of congestus cloud decks at such latitudes [11]. In this study we include the effect of rotation to see whether rotation will change this picture and especially whether rotation alone will have such an effect on organized convection.

For the sake of completeness and for consistency with the nonlinear and stochastic simulations presented in Section 5, in addition to the KM08 parameter regime [18] we also consider the "deterministic" parameter regime of [3] presented on purpose in that paper as the regime where the performance of the multicloud model is deficient. It is referred here as the FMK13 parameter regime. The KM08 and FMK13 parameters are summarized in Table 2. We note that the main differences between these two regimes are found in the key convective and congestus parameters a_0 and γ'_2. In [2,3], we showed that the introduction of the stochastic model drastically improves the behavior of the nonlinear dynamics of convectively coupled waves and of the mean climatology for the FMK13-deficient regime.

In Figure 1, we present the linear stability diagrams for the KM08 and FMK13 regimes when both the Coriolis and atmospheric dryness parameters are varied. As we see from the two panels (a) and (b), in the KM08 regime increasing the Coriolis parameter has the same effect on the stability features of the multicloud model as increasing the atmospheric dryness. In both cases, the main MGWI fades out and is replaced by the instability of a standing-congestus mode, which is extensively documented in [18]. This is perhaps a mere coincidence but the main conclusion here is that in nature both rotation effects and atmospheric dryness are believed to play an important role in confining congestus cloud decks to higher latitudes while the moist and rotationless equatorial region is more favorable for organization of deep convection [22]. While the same fading of the MGWI occurs also in the FMK13 cases displayed in Figure 1 (c) and (d), this regime does not have a congestus-standing mode instability due to the small value of the congestus parameter γ_2' used here.

The effect of rotation on the unstable modes in the KM08 regime is further documented in Table 3. Two additional features are worth noting here. 1) As the Coriolis parameter increases the phase speed of the moist gravity waves gradually increases to approach and then exceed that of the dry second baroclinic gravity wave of ≈ 25 m/s while their growth rate decreases and ultimately become stable. 2) The instability band of the congestus mode widens toward smaller scales with increasing Coriolis parameter while its maximum growth remains at large sales. This growth rate is controlled solely by atmospheric dryness; it remains below 0.001 1/day for $\overline{\theta}_{eb} - \overline{\theta}_{em} = 11$ K and below 0.135 1/day for $\overline{\theta}_{eb} - \overline{\theta}_{em} = 14$ K. This is consistent with the idea that both the Coriolis parameter and atmospheric dryness play a role in confining congestus cloud decks to higher latitudes but suggests that their strength is controlled by the gradient of θ_e.

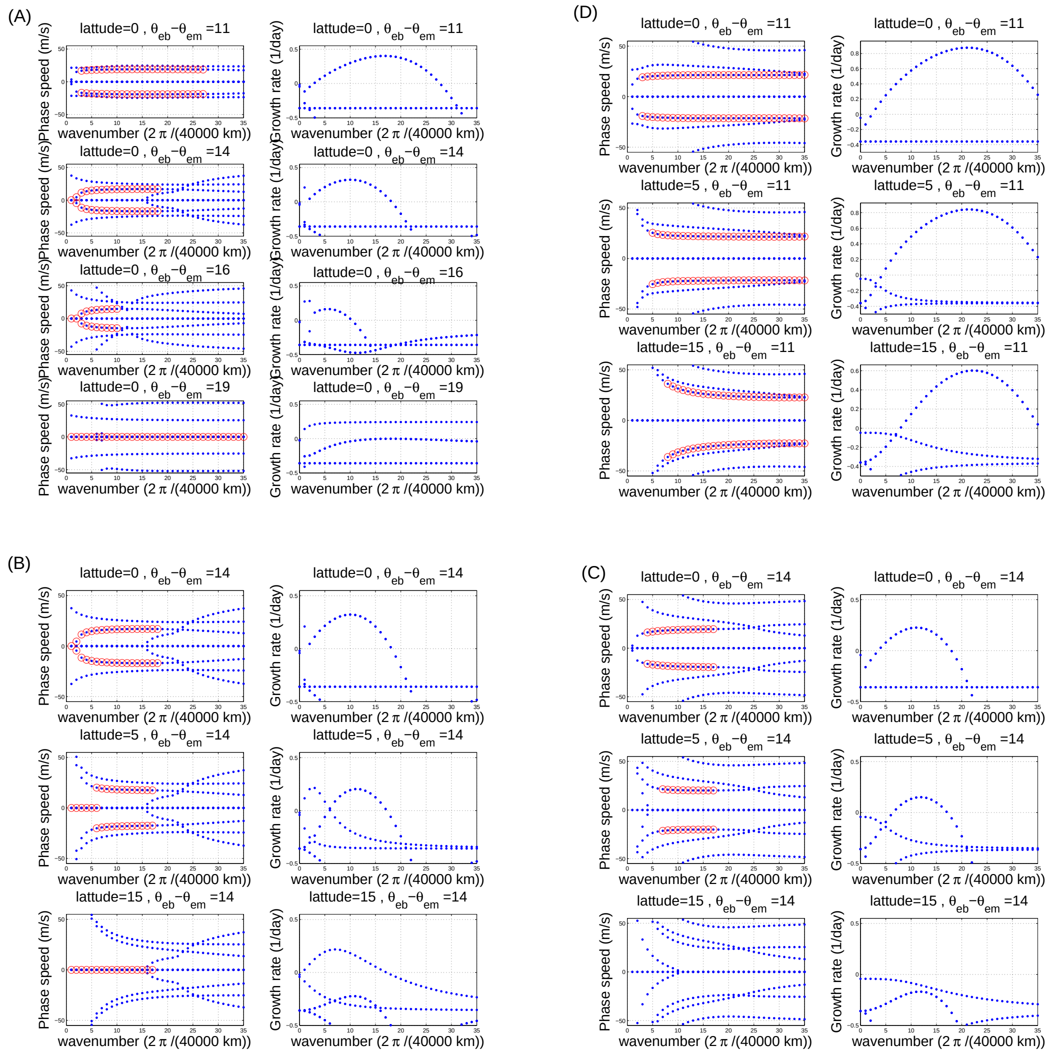

Fig. 1 Effect of rotation and atmospheric dryness on the linear stability diagram for the KM08 and FMK13 parameter regimes. (a) KM08, $\phi_y = 0, \bar{\theta}_{eb} - \bar{\theta}_{em} = 11, 14, 16, 19$ K, (b) KM08, $\phi_y = 0, 5, 15^o$, $\bar{\theta}_{eb} - \bar{\theta}_{em} = 14$ K, (c) FMK13 $\phi_y = 0, 5, 15^o$, $\bar{\theta}_{eb} - \bar{\theta}_{em} = 14$ K, (d) FMK13 ϕ=$0, 5, 15^o$, $\bar{\theta}_{eb} - \bar{\theta}_{em} = 11$ K

To elucidate some of the plausible physics that control the change in behavior of convectively coupled waves, in Figure 2 we show the bar diagrams corresponding to three latitudes 0,5, and 10 degrees for the KM08 regime with $\bar{\theta}_{eb} - \bar{\theta}_{em} = 14$ K. As expected, the nonzero Coriolis parameter induces a

Table 3 Effects of rotation on unstable modes for KM08 regime.

		Moist gravity wave				Standing-Congestus mode		
$\overline{\theta}_{eb} - \overline{\theta}_{em}$	Latitude (degrees)	Most unstable mode	Phase Speed (m/s)	Growth rate (1/day)	Range of Instability	Most unstable mode	Growth rate (1/day)	Range of Instability
11	0	17	19.17	0.393	2-28	–	–	–
	2.5	17	19.3	0.382	5-28	1	- 0.0046	–
	5	11	19.7	0.35	6-27	1	10^{-6}	1
	7.5	11	20.3	0.301	7-26	2	0.001	1
	10	11	21.0	0.241	9-25	2	0.0004	1
	15	10	23.1	0.099	11-23	4	0.0006	3-4
	20	10	26.4	-0.05	–	5	0.001	4-5
14	0	10	16.6	0.32	2–21	1	0.13516	1
	2.5	10	17.6	0.24	4-17	2	.1214	1-2
	5	11	18.3	0.2	5-16	3	0.1328	1-4
	7.5	12	20.2	0.06	8-14	4	0.1345	1-7
	10	10	22.9	-0.05	–	5	0.13502	1-10
	20	10	35.6	-0.36	–	9	0.13557	1-18

nonzero meridional (cross-equatorial) velocity components, v_1, v_2, that may significantly modify the dynamics of these waves. As highlighted in the caption of Figure 2, the combined relative strength of v_1, v_2 reaches roughly 50% of that of (u_1, u_2) at $\phi_y = 5$ degrees and increases to about 70% at $\phi_y = 10$ degrees. A close look at the three bar diagrams in Figure 3 reveals that during the growth of (v_1, v_2), the relative strengths of u_1, u_2 and the other diagnostic variables remain constant at the expense of the moisture component q which diminishes considerably in strength as the Coriolis parameter is increased, although this moisture component remains the dominant one. This decrease in the moisture component perhaps explains both the reduced instability and the increased phase speed as the Coriolis parameter is increased.

Another important physical effect implied by rotation is a significant modification of the dispersion relations of the underlying gravity waves. As highlighted below, the nonzero f makes the moist gravity waves more dispersive

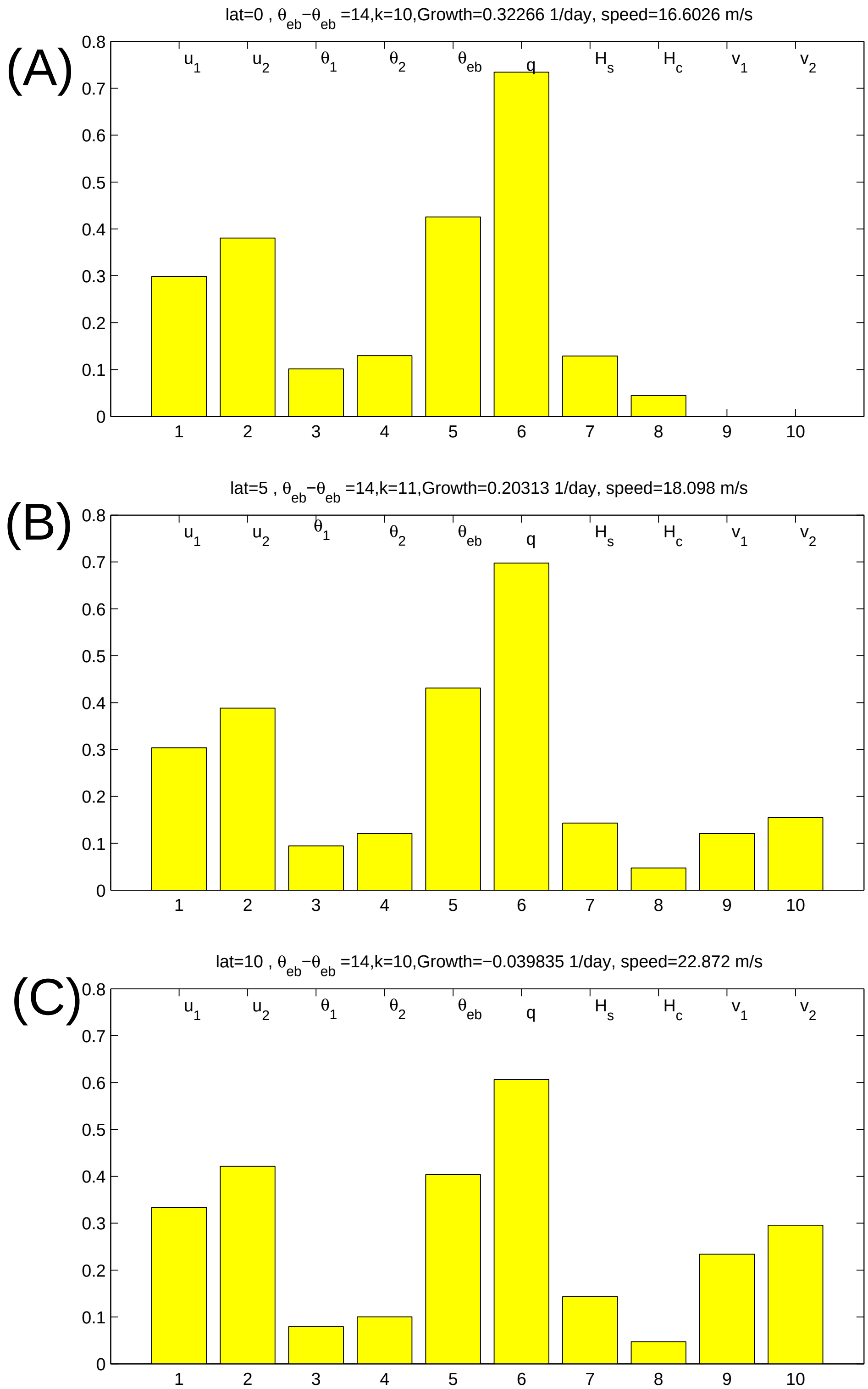

Fig. 2 Bar diagrams showing the relative strengths of the prognostic variables for the most unstable moist gravity waves in the KM08 regime with $\theta_{eb} - \bar{\theta}_{em} = 14$ K and a) $\phi_y = 0$, b) $\phi_y = 5$ degrees, and c) $\phi_y = 10$ degrees.

and more in line with the traditional Poincare waves on an f-plane, unlike the case $f = 0$ which results in waves that look more like Kelvin waves. In fact, plugging the usual ansatz

$$\begin{pmatrix} u_j \\ v_j \\ \theta_j \end{pmatrix} = e^{i\omega(k)t-kx} \begin{pmatrix} \hat{u}_j \\ \hat{v}_j \\ \hat{\theta}_j \end{pmatrix}, j = 1, 2$$

in (2), where $i^2 = -1$, and ignoring the heating and cooling and moisture coupling etc. yields the dispersion relation

$$\omega(k) - \frac{k^2}{j^2}\frac{1}{\omega(k) - i/\tau_D} - \frac{f^2}{\omega - id} - di = 0,\ j = 1, 2.$$

For high frequency waves, so that $1/\tau_D, d \ll 1$, this reduces to

$$w^2 = f^2 + k^2/j^2,\ j = 1, 2$$

which is essentially the dispersion relations of f-plane Poincare waves. Notice also general identity

$$\hat{v}_j = i\frac{f}{\omega - id}\hat{u}_j, \tag{5}$$

for linearized waves regardless of moisture coupling, which again suggests that high frequency waves are such that the meridional velocity anomalies are (almost) in quadrature with the zonal velocity anomalies as for Poincare waves. This is in fact confirmed in Figure 3 (a) where we plot the zonal structure of the zonal and meridional velocity components of the most unstable moist gravity waves in the KM08 regime at 10 degree latitude and for $\theta_{eb} - \bar{\theta}_{em} = 14$ K. This is contrasted with the structure of the standing congestus mode in Figure 3 (b), which as expected does not appear to have this quadrature prop-

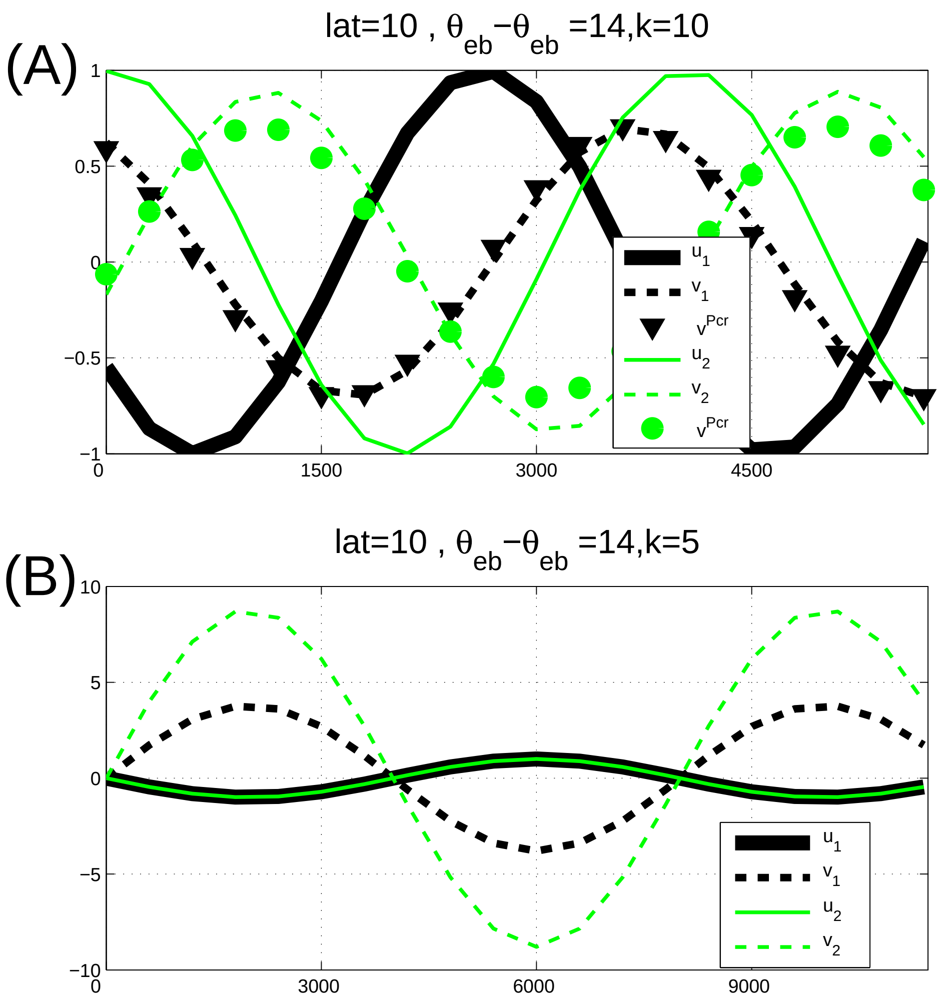

Fig. 3 (a) The structure of the zonal and meridional velocity components of the most unstable moist gravity waves in the KM08 regime at 10 degree latitude and for $\theta_{eb} - \bar{\theta}_{em} = 14$ K. v^{Pcr} is the meridional velocity component of the corresponding dry Poincare wave. (b) The structure of the zonal and meridional velocity components of the most unstable standing-congestus mode in the same parameter regime.

erty because meridional and zonal velocities are anti correlated as predicted by (5) when ω is pure imaginary and $i\omega - id < 0$.

In Table 4, we report the strength of the dynamical terms in the θ equation for the unstable moist gravity wave (MGW) and congestus modes in the KM08 parameter regime to assess whether any of these modes are WTG. We do this for the first and second baroclinic modes separately. As we can see from this table the time derivative of the first baroclinic components of the MGW mode is roughly one order of magnitude smaller than the other dynamical terms. The corresponding quantities for the congestus mode are relatively higher than that but they remain (4 to 5 times) smaller compared to the corresponding other dynamical terms. However, for both modes, the second baroclinic components are comparable in magnitude to the other dynamical terms. This suggests that, for tropical wave dynamics, the WTG approximation is valid for convectively coupled gravity waves in their first baroclinic component but its generalization to the whole dynamics (i.e to shallower vertical modes) is questionable. The systematic derivation of the WTG models from [31] presented in [25] relies on the smallness of the Froude number, the ratio of the typical velocity to the gravity wave speed; second baroclinic dry gravity waves move at half the wave speed of the first baroclinic mode gravity waves and therefore have a larger Froude number. Evidently, moisture coupling with larger Froude number invalidates the ”simple” WTG approximation [31] here for the second baroclinic component. Fortunately, there are a wide variety of generalized multi-scale WTG approximations [24, 25, 19] which also allow for suitable gravity wave dynamics and ameliorate this difficulty with the original WTG approximation from [31].

4 Effect of rotation and atmospheric dryness on organized convection and mean circulation

In this section we present long run nonlinear simulations using both the deterministic and stochastic multicloud models which we interpret in the light of the linear analysis presented above and try to gain some more understanding

Table 4 Strength of the dynamical terms for the most unstable moist gravity wave (MGW) and congestus mode in the KM08 parameter regime at 5 degrees. See text for details.

First Baroclinic

	Moist gravity wave		
latitude (degrees)	$\|\|i\omega\hat{\theta}_1\|\|$	$\|\|ik\hat{u}_1\|\|$	$\|\|\hat{H}_d + \xi_s \hat{H}_s + \xi \hat{H}_c - \hat{\theta}_1/\tau_D\|\|$
0	0.0785	0.7002	0.6299
5	0.0869	0.7844	0.7036
10	0.0978	0.9078	0.8126
15	0.0971	0.9268	0.8302
	Congestus mode		
0	0.0061	0.0243	0.0306
5	0.0076	0.0572	0.0651
10	0.0074	0.0458	0.0535
15	0.0072	0.0409	0.0483

Second Baroclinic

	Moist gravity wave		
latitude (degrees)	$\|\|i\omega\hat{\theta}_2\|\|$	$\|\|ik\hat{u}_2/4\|\|$	$\|\|\hat{H}_c - \hat{H}_s - \hat{\theta}_2/\tau_D\|\|$
0	0.1002	0.2234	0.1393
5	0.1111	0.2506	0.1515
10	0.1223	0.2836	0.1664
15	0.1168	0.2786	0.1628
	Congestus mode		
0	0.0241	0.0241	0.0489
5	0.0142	0.0266	0.0413
10	0.0172	0.0265	0.0442
15	0.0186	0.0263	0.0455

of the properties of organization of convection in the tropics and extra-tropics. As we will see below, the stochastic simulations have strong qualitative resemblance with the CRM simulations of Liu and Moncrieff [22] on a $4,000$ km domain.

The governing equations in (2) and Table 1 are solved numerically for about 500 days, starting from a random initial condition. After a short transient period of less than 100 days the solution enters a statistical steady state. For each one of the three cases presented below, we plot the spatial structure of the time mean, discarding the transient period, and the Hovmöller diagrams of deviations from this mean to separate the climatological-mean circulation due to steady forcing and/or standing modes from propagating waves. More details on the procedure including details of the simulations can be found in [16,18].

4.1 Deterministic simulations: Homogeneous SST

We consider a homogeneous SST background, i.e, the imposed sea surface evaporative forcing $\theta^*_{eb} - \bar{\theta}_{eb}$ and all other model parameters assume their values in Tables 1 and 2, for the KM08 regime. In Figure 4 (a),(b),(c), (d) we show the time averaged zonal and meridional structure of the velocity components, heating rates H_d, H_s, H_c, moisture anomalies q, and the zonal circulation patterns with $u - w$ velocity arrows overlaid on top of potential temperature contours corresponding respectively to latitudes $\phi_y = 2.5, 5, 10, 20$ degrees. As we can see from Figure 4(a),(b),(c), although the external forcing is uniform a nontrivial mean solution develops for all three latitude cases. This is in fact a manifestation of the standing-congestus mode of linear instability, identified in Section 3, as rotation and dryness effects are increased. Consistently, this mean solution is characterized by a dominating congestus heating characterized by moist and dry regions separated by high congestus gradients and substantial peaks in velocity amplitudes. Also, consistent with linear theory, those gradients become sharper and sharper as the Coriolis parameter is increased because of the spread of the large scale instability to smaller scales. The case $\phi_y = 20$ degrees is even more revealing as it shows a wavy pattern with a clear wavenumber $k = 4$ unlike the cases in (a),(b), and (c) that display a double-cell Walker type circulation as suggested in [18] for the case $f = 0$. Moreover, the overall amplitude of the solutions in Figure 4 remains unchanged except for the meridional velocity which increases considerably with rotation. This is consistent with the fact that linear theory predicted a growth

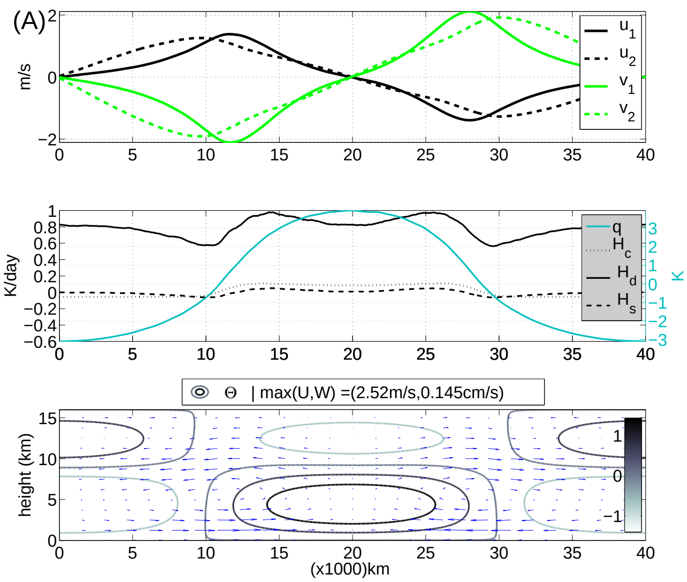

Fig. 4 Time averaged zonal and meridional velocity components (top), heating rates and moisture (middle), and mean zonal circulation patterns (bottom) for the MK08a parameter regime with a uniform SST background: (a) $\phi_y = 2.5$ degrees.

rate for the congestus mode which is independent of rotation and the zonal mean circulation is roughly constant in magnitude so the first equation in (4) predicts a meridional mean flow strongly increasing with rotation. Also the u and v components are anti-correlated to each other as predicted by linear theory using (5) with imaginary frequency.

In Figure 5 (a) and (b), we plot the Hovmöller diagrams (x-t contours) of the wave fluctuations from the mean solutions presented in Figure 4 for the two cases corresponding to $\phi_y = 2.5$ and 5 degrees, respectively. Interestingly on top of the standing-congestus mode, we see moist gravity waves moving in both directions at roughly 18 m/s evolving mainly within the moist region with the congestus-standing mode acting as a barrier trying to confine convective organization, as already noted in [18]. It is also worth noting that as expected,

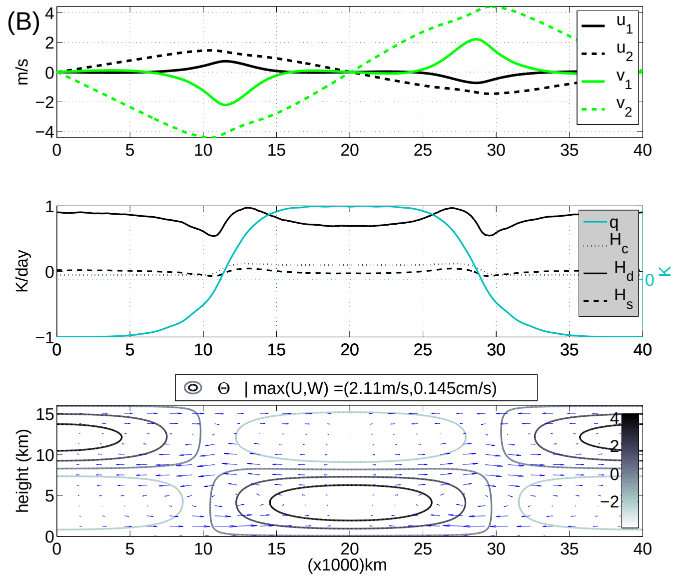

Figure 4 (continued): (b) $\phi_y = 5$ degrees.

due to the Coriolis effect, the moist gravity waves carry a nontrivial meridional velocity v (not shown here) which is in quadrature with the zonal velocity u and whose amplitude increases with f. For higher Coriolis forcing $\phi_y \geq 7$ the wave fluctuations are very weak and when $\phi_y \geq 10$ the solution becomes steady; consistent with the linear theory results in Section 3 it is dominated by the standing-congestus mode, which eventually saturates due to nonlinear effects.

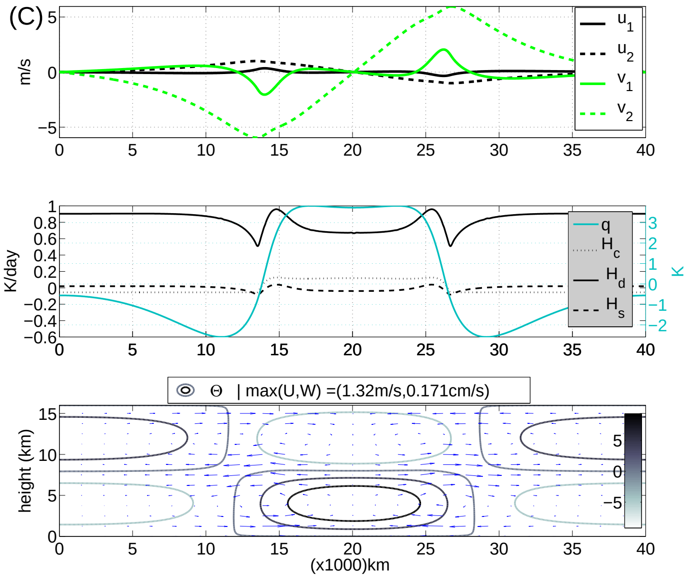

Figure 4 (continued): (c) $\phi_y = 10$ degrees.

362 4.2 Deterministic simulations: Warm pool forcing

We now introduce a non-homogeneity in the surface forcing by modifying the evaporative flux to mimic the maritime continent warm pool. We set

$$\theta^*_{eb} - \bar{\theta}_{eb} = \begin{cases} 10\cos(x - x_0) \text{ K} & \text{if } |x - x_0| < \pi/2 \\ 5 \text{ K} & \text{otherwise,} \end{cases} \tag{6}$$

363 so that the surface heating and moistening is raised by 5 degrees in the centre
364 of the warm pool and lowered by 5 K outside, with respect to the uniform
365 background used before.

366 In Figure 6 we show the mean circulation patterns obtained with the warm
367 pool simulations for the case $\phi_y = 0$ and $\phi_y = 5$ degree in the KM08 parameter
368 regime. As expected from (4), as we go from the equator to higher latitudes,

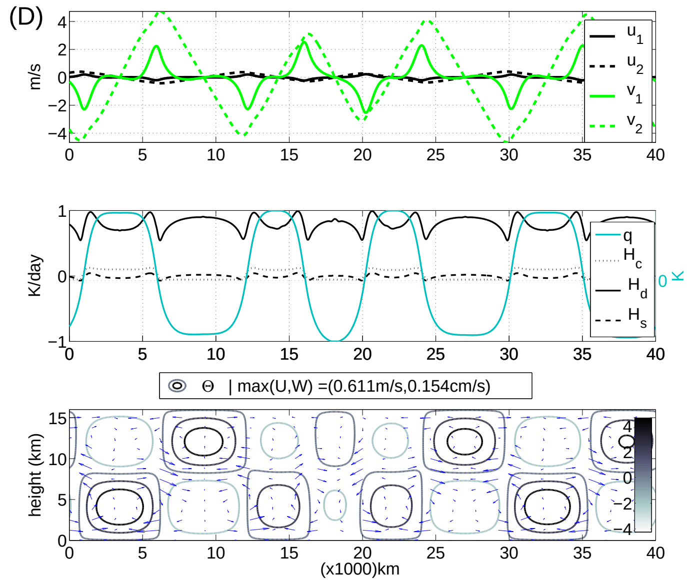

Figure 4 (continued): (d) $\phi_y = 20$ degrees.

the meridional mean circulation increases in strength. As we move from the equator to higher latitudes, the Walker circulation transitions from a deep first baroclinic circulation to a shallower one which is characterized by a mid-level jet reminiscent of a strong second baroclinic component due to the congestus mode which dominates the heating field. This is in fact very similar to the homogeneous RCE case. Compare Figure 6(b) with Figure 4(b). As f is increased, the congestus-standing mode develops and aligns itself with the warm pool geometry. Note that the situation is different at much higher f values as we are not getting a packet of standing waves any more because the warm pool forcing provides a preferential location for the congestus mode. However, the zonal Walker-cell circulation becomes much weaker and more confined to the warm pool region as f is increased. The sudden transition of the Walker circulation from deep to shallow reminiscent of the mixed-type secondary shallower

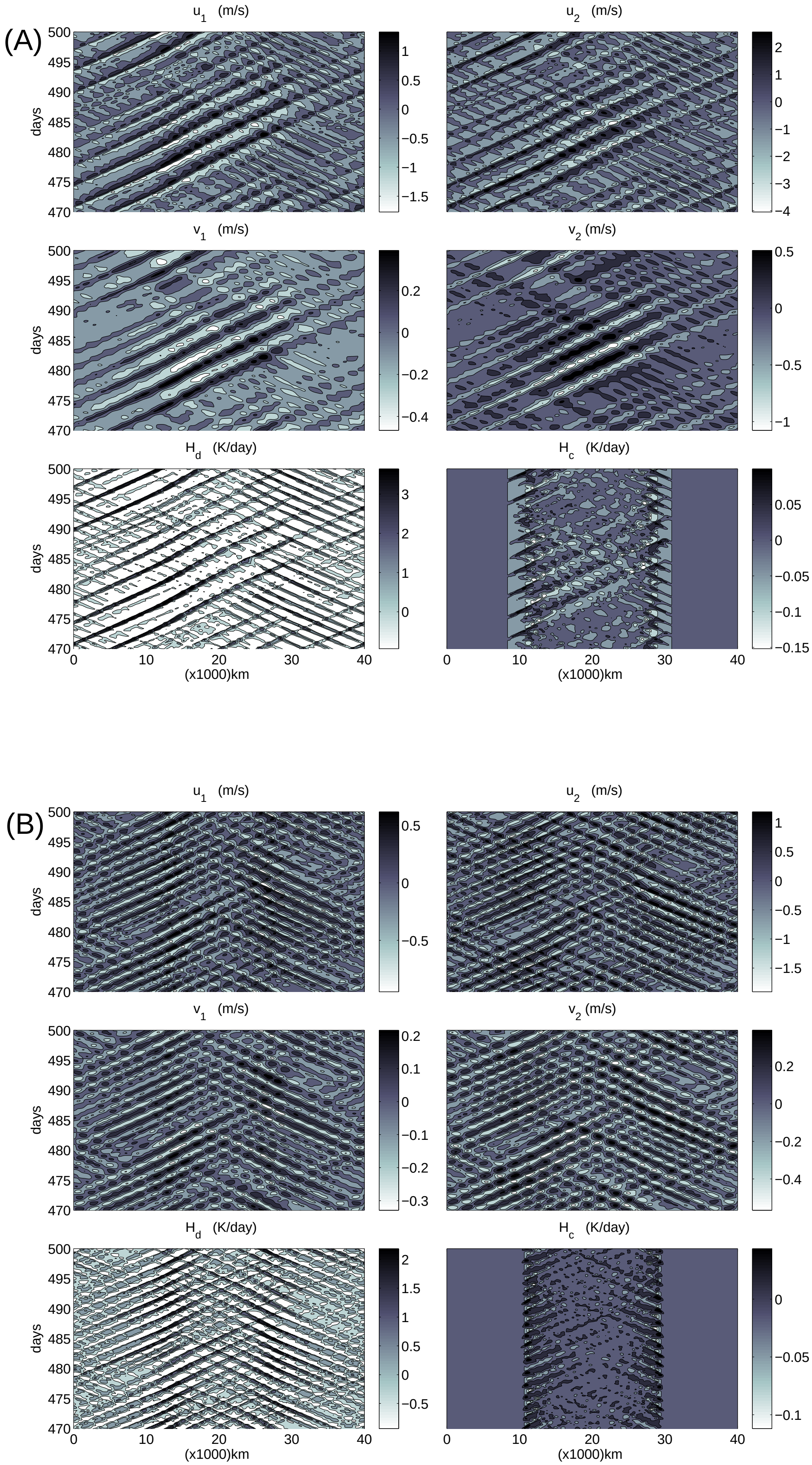

Fig. 5 Hovmöller diagrams (x-t contours) of the wave fluctuations corresponding to the mean solutions presented in Figure 4. First and second baroclinic zonal velocities (top left and top right), first and second baroclinic meridional velocities (middle left and middle right

circulation observed at higher latitudes in the mean monsoonal circulation [29] while the confinement of the subsiding circulation to the vicinity of the heating source is consistent with the findings of Liu and Moncrieff [22].

Figure 7 shows the wave fluctuations associated with the warm pool simulations in Figure 6. As expected the strong convectively coupled gravity waves seen in the case without rotation in (a) weaken substantially as the rotation is introduced and they become very confined to the edges of the warm pool; moist gravity waves seem to be initiated at the warm pool centre and amplify at its edges as they propagate in both directions and then fade out and die when they leave the moist region. The same confinement of convection seen in Figure 5 (to the centre of the standing congestus mode) seems to operate here also.

4.3 Stochastic simulations

In this section we couple the multicloud equations in (2) to a stochastic model for the area fractions of the three main cloud types represented by the model: congestus, deep, and stratiform. The stochastic multicloud model (SMCM) is designed in [13] to account for the missing subgrid scale variability of convection in GCMs. It is successfully used in [2,3] for the simulation of convectively coupled waves and tropical climate in the context of the crude vertical resolution model in (2).

As in the deterministic simulations reported above, we also consider here both the cases of a uniform and a warm pool SST backgrounds but for the FMK13 parameter regime. First, we recall that the linear (deterministic) theory, from Section 3, exhibits, in this regime, a systematic decrease in growth rates of the synoptic scale instability of moist gravity waves as the Corio-

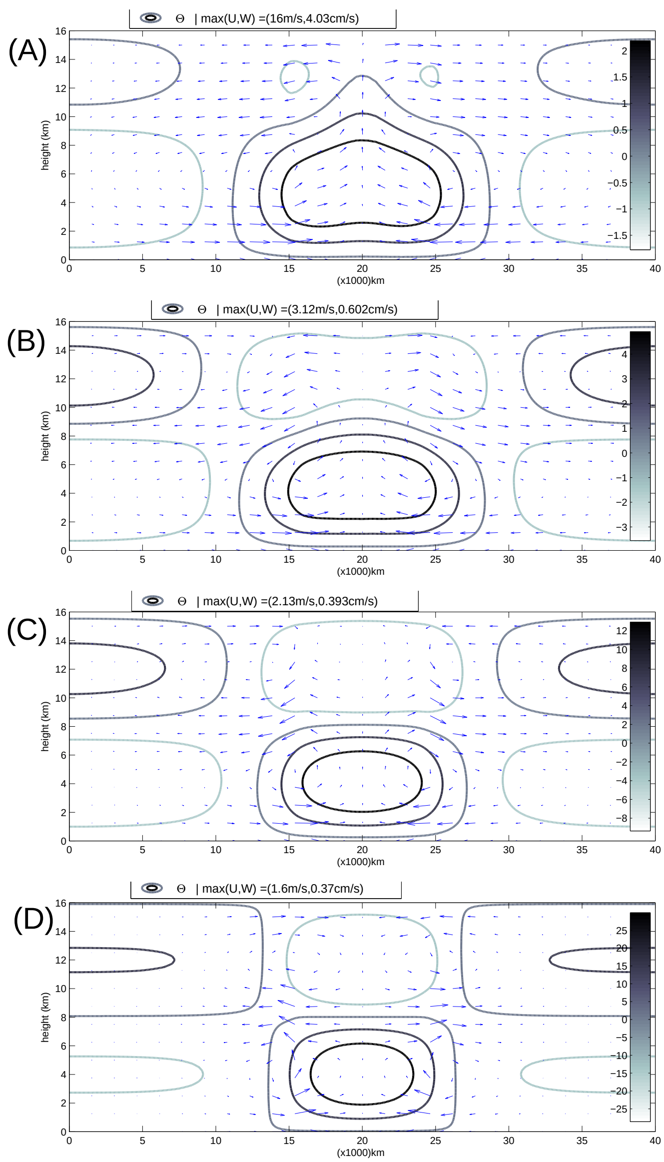

Fig. 6 Mean zonal circulation patterns for the MK08 parameter regime with a warm pool SST: (a) $\phi_y = 0$ degrees, (b) $\phi_y = 5$ degrees, (c) $\phi_y = 10$ degrees, (d) $\phi_y = 20$ degrees.

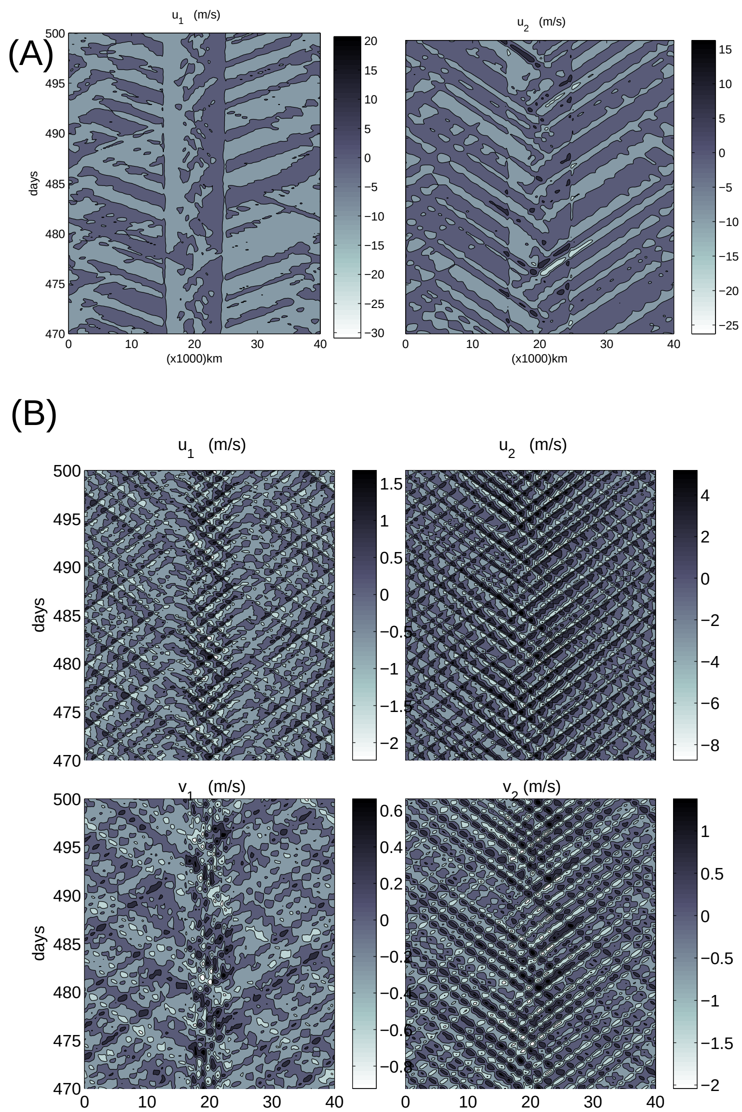

Fig. 7 Zonal and meridional velocities of wave disturbances associated with the warm pool simulations in Figure 6. (a): Equator, $\phi_y = 0$ (meridional velocities are zero in this simulation, thus only zonal velocities are plotted), (b) $\phi_y = 5$ degrees.

lis parameter is increased but they remain unstable even at $\phi_y = 20^o$, when $\bar{\theta}_{eb} - \bar{\theta}_{em} = 11$ K. However, when $\bar{\theta}_{eb} - \bar{\theta}_{em} = 14$ K, the instability fades out somewhere between 5 and 15^o. At $\bar{\theta}_{eb} - \bar{\theta}_{em} = 14$ K, (results not shown) the model becomes stable at 5^o. In all cases, the FMK13 regime does not develop a congestus mode instability as f is increased. By choosing to couple the SMCM to the model in (2) we can address the important question of whether with the help of the stochastic parametrization, the multicloud model can reproduce some of the behavior seen in the deterministic simulations such as the weakening and confinement of the moist gravity waves and Walker circulations even though a congestus mode instability is lacking. Moreover, we can address the important question of whether the SMCM will be capable of reproducing the CRM behavior seen in [22] such as the "disorganization" and patchiness of convection that occurs at high Coriolis parameter values. Recall that in the deterministic simulations, the congestus mode instability, is suggested to help establish the confinement of moist gravity waves in the deterministic simulations.

In a nutshell, the coarse-grained SMCM [13, 2, 3] is a probabilistic model for the area fractions of congestus, deep, and stratiform cloud types, denoted here σ_c, σ_d and σ_s, respectively. A rectangular lattice of $N = n \times n$ sites is overlaid over each GCM horizontal grid. Here we assume $n = 20$ so that for a large-scale resolution of 40 km the lattice sites are 2 km apart from each other. Let N_c, N_d, N_s be the number of lattice site that are occupied by a congestus, deep, and stratiform cloud types, respectively. The triplet form a three dimensional birth and death process with immigration, that is, cloud populations can increase by the birth of new cloudy sites, decrease by the death of older ones, or exchange members by transitions of some sites from one cloud type to another. It forms an ergodic Markov process with a well defined limiting distribution which depends only on the large scale (GCM) variables. In the SMCM, we as-

Table 5 Transition time scales for the SMCM simulations [3]. See text for details.

Transition	Rate	Time scale (hours)
Clear to congestus	$R_{01} = \Gamma(D)\Gamma(C_l)/\tau_{01}$	τ_{01} =1
Clear to deep	$R_{02} = [1 - \Gamma(D)]\Gamma(C)/\tau_{02}$	$\tau_{02} = 3$
Congestus to deep	$R_{12} = (1 - \Gamma(D))\Gamma(C)/\tau_{12}$	$\tau_{12} = 1$
Deep to stratiform	$R_{23} = 1/\tau_{23}$	$\tau_{23} = 3$
Congestus to clear	$R_{10} = 1/\tau_{10}$	τ_{10} =1
Congestus to clear	$R_{20} = 1/\tau_{20}$	$\tau_{20} = 3$
Congestus to clear	$R_{30} = 1/\tau_{30}$	$\tau_{30} = 5$

sume that, under very specific large scale conditions, only congestus and deep sites can be created from clear sky sites and that a congestus site can transit to a deep site and a deep site can transition to a stratiform site. Any cloudy site can decay into a clear sky site. A single transition time scale $\tau_{kj}, k, j = 0, 1, 2, 3$ is associated with each one of these seven state transitions of the lattice sites. The closure equations of the transition rates and the values of the transition time scales used for this article are given in Table 5 [3]. The transition rates are defined in terms of midtropospheric dryness $D = (\theta_{eb} - \theta_{em})/T_0$, normalized values of convective available potential energy, CAPE/CAPE$_0$, and low level CAPE, $CAPLE_l/CAPE_0$, through an Arrhenius-type activation function: $\Gamma(x) = 1 - e^{-x}$ if $x \geq 0$ and $\Gamma(x) = 0$ if $x < 0$. Here $T_0 = 10$ K and $CAPE_0 = 2000$ J/kg. Also the physical constant R used to define CAPE and CAPE$_l$ in Table 1 take the value $R = 2.1514e-04J/kgK^-1$[13]. The coupling of the SMCM to the large-scale equations is summarized in Table 1 and the interested reader is referred to the original papers [13,2,3] for details. There is a recent generalization of SMCM to allow for local interactions [12] .

As in the deterministic simulation we run the coupled SMCM model for 400 days using a 2 minute time step and a 40 km grid spacing combined with a lattice size of 20×20 microscopic sites per grid cell. In Figure 8(A),(B), and(C), we plot the Hovmöller diagrams for the deep and congestus area fractions, a surrogate for convective cloud cover, obtained by SMCM simulations

Table 6 Time series variance for SMCM simulations with homogeneous SST background.

$\bar{\theta}_{eb} - \bar{\theta}_{em}$	Variable (Units)	Equator	5^o	10^o	20^o
11 K	u_1, u_2 (m/s)^2	9.0, 6.5	2.5, 4.3	1.0 ,3.5	0.5 , 3
	v_1, v_2 (m/s)^2	0,0	0.5, 1.0	4.5, 1.5	3.5 , 2.5
	q K^2	6.4	3.6	2.1	1.4
14 K	u_1, u_2 (m/s)^2	9.5, 6.5	2.0, 4.5	1.0, 4.0	0.5, 3.5
	v_1, v_2 (m/s)^2	0,0	4.5, 0.5	5.0, 2.0	6.0, 3.0
	q K^2	6.5	2.9	2.2	1.7

with homogeneous SST at latitudes 0, 5, and 20 degrees, respectively when $\bar{\theta}_{eb} - \bar{\theta}_{em} = 11$ K. As noted in [3], at the equator (0 latitude) the SMCM exhibits synoptic to planetary wave envelopes of mesoscale propagating convective signals with appreciable variance. As we see in Figure 8, as the Coriolis effect is introduced and increased this synoptic to planetary scale organization weakens and disappears. It is gradually replaced by chaotic and somewhat patchy convective events. In Table 6 we report the variability in horizontal and meridional velocity components and moisture anomaly fields for the cases of Figures 8 and 9. We note from Table 6 that in addition to the patchiness of convection, the whole zonal wave fluctuations get attenuated as f is increased while the meridional component of the variance increases substantially. This is consistent with the linear theory results of Section 3. The more patchy and less organized cases correspond to the linearly stable regimes. This patchiness or rather lack of organization thereof is qualitatively similar to what is observed in the CRM simulations of Liu and Moncrieff [22]; see Figures 7 and 8 from [22] and compare with our Figures 8 and 9. The analogy is even more evident in the warm pool simulations presented next.

In Figures 10, 11,12, we plot the mean/Walker circulation patterns obtained by SMCM simulations with 5 K warm pool SST forcing (6) using the FMK13 parameter regime with $\bar{\theta}_{eb} - \bar{\theta}_{em} = 10, 14, 20$ K, respectively; the Coriolis parameter is increased from 0 to its value at $\phi_y = 20^o$. The wave and

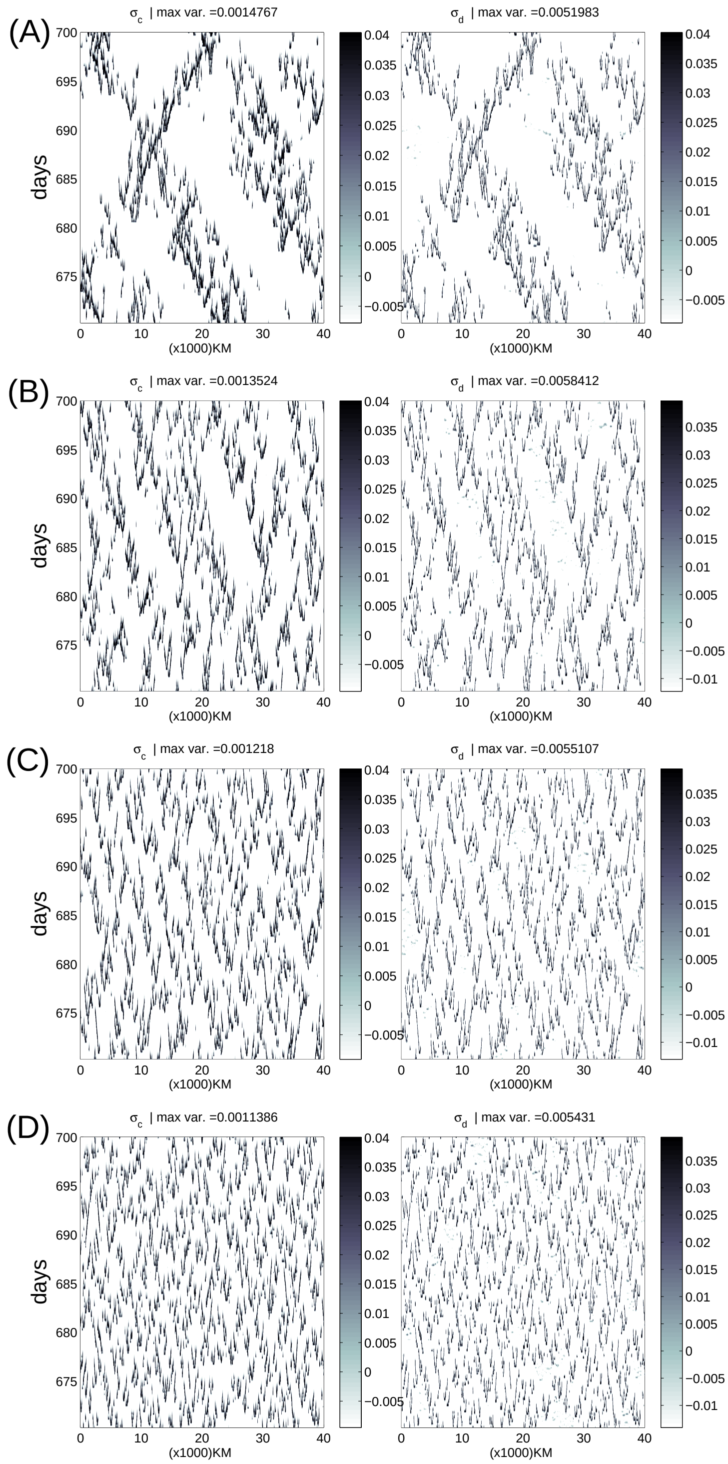

Fig. 8 Hovmöller diagram of the area fractions of congestus (left) and deep (right) cloud types for SMCM simulations using a uniform SST and $\bar{\theta}_{eb} - \bar{\theta}_{em} = 11$ K. (a) Equator, (b) 5^0, (c) 10^o. and (d) 20^o.

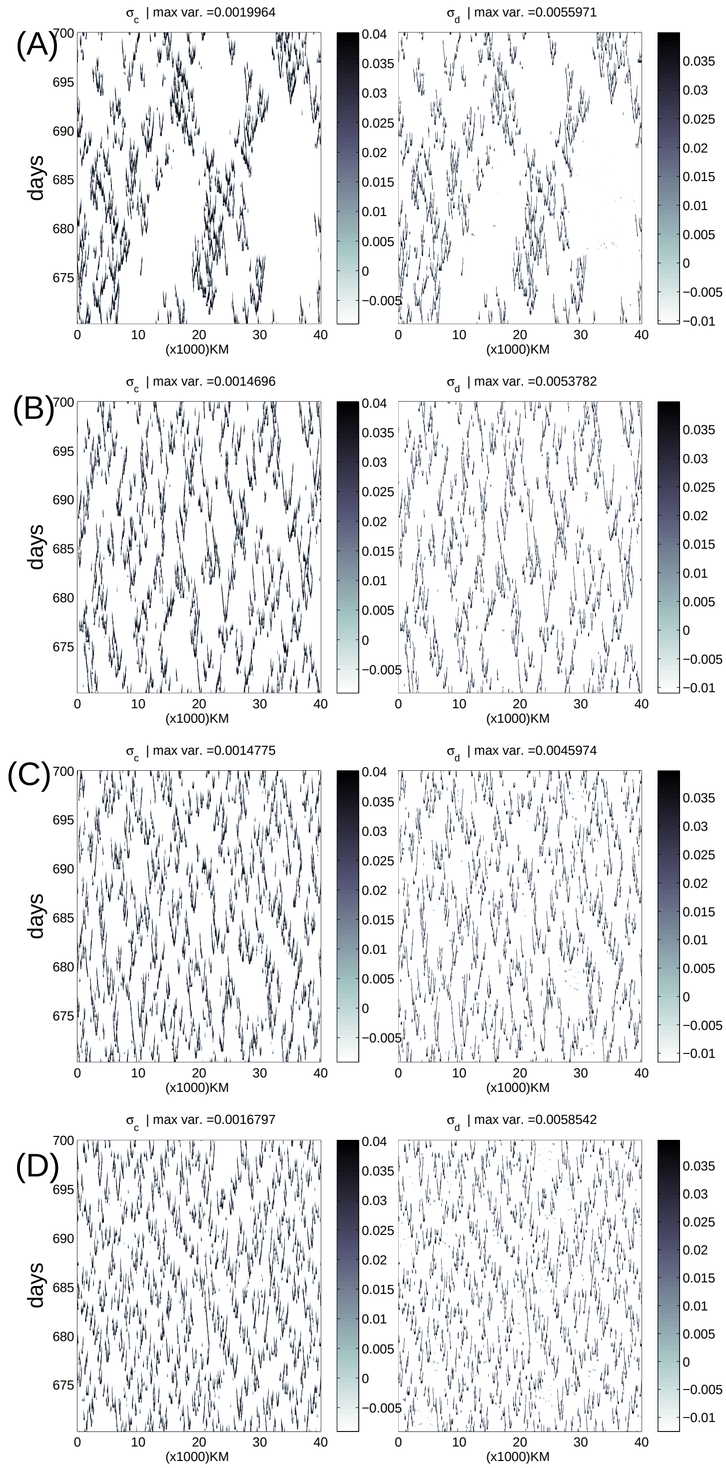

Fig. 9 Same as Figure 8 but for $\bar{\theta}_{eb} - \bar{\theta}_{em} = 14$ K. (a) Equator, (b) 5^0, (c) 10^o, (d) 20^o.

Table 7 Strength of mean zonal circulation (U m/s, W cm/s) for the warm pool SMCM simulations using the FMK13 regime.

Latitude	$\theta_{eb} - \theta_{em} = 10$ K	$\theta_{eb} - \theta_{em} = 14$ K	$\theta_{eb} - \theta_{em} = 20$ K
0^o	8.6, 2.7	11.1, 1.3	11.8, 3.2
5^o	3.0, 0.6	3.0, 0.7	3.8, 0.8
10^o	1.3, 0.4	1.2, 0.5	1.1,0.6
20^o	0.6, 0.4	0.5 , 0.4	0.8 , 0.4

convective fluctuations behave similarly as in the homogeneous SST simulations reported in Figures 8 and 9, except that they are now more confined to the warm pool region [2,3]. In Tables 7 and 8, we display the actual strengths of the mean and fluctuations, respectively. Similarly to both the homogeneous SST and deterministic simulations, we see a significant decrease in strength of the zonal mean circulation and variability and confinement of the mean circulation to the warm pool consistent with the findings of Liu and Moncrieff [22]. This confinement is further accelerated with the increase in atmospheric dryness parameter $\bar{\theta}_{eb} - \bar{\theta}_{em}$. However, the mean circulation in Figures 10, 11, and 12 does not become significantly shallow with increasing f as in the case of the deterministic simulations using the KM08 regime in Figure 6. This supports the claim that the transition to a shallower mean circulation in Figure 6 is mainly controlled by the congestus mode instability, since it is absent in the FMK13 regime as reported in Figure 1. Moreover, while the zonal means $\langle u \rangle_1, \langle u \rangle_2$ decrease significantly with f, the strength of the meridional means $\langle v \rangle_1, \langle v \rangle_2$ remains roughly unchanged, as f is increased from 5 to 20^o, except for the case $\bar{\theta}_{eb} - \bar{\theta}_{em} = 20$ K where $\langle v \rangle_{1,2}$ seem to decrease with f but they remain substantially larger than $\langle u \rangle_{1,2}$. This can be explained from Equation (4) by the fact that the drastic decrease in $\langle u \rangle_1, \langle u \rangle_2$ is compensated by the increase in the value of f.

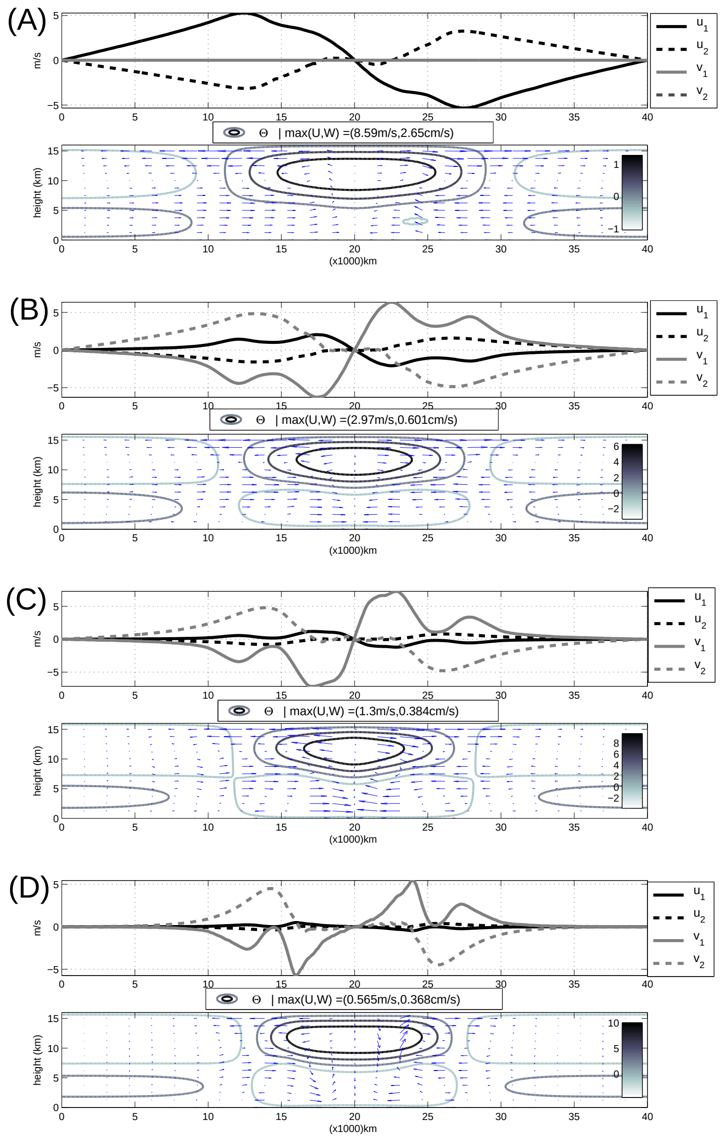

Fig. 10 Walker circulation patterns obtained by SMCM simulations on a 5 K warm pool SST forcing using the FMK13 parameter regime with $\bar{\theta}_{eb} - \bar{\theta}_{em} = 10$ K. (a) Equator, (b) 5^0, (c) 10^o, (d) 20^o. Top panel of each subplot shows the time averaged zonal and meridional velocities, while the mean zonal circulation pattern is given in the bottom.

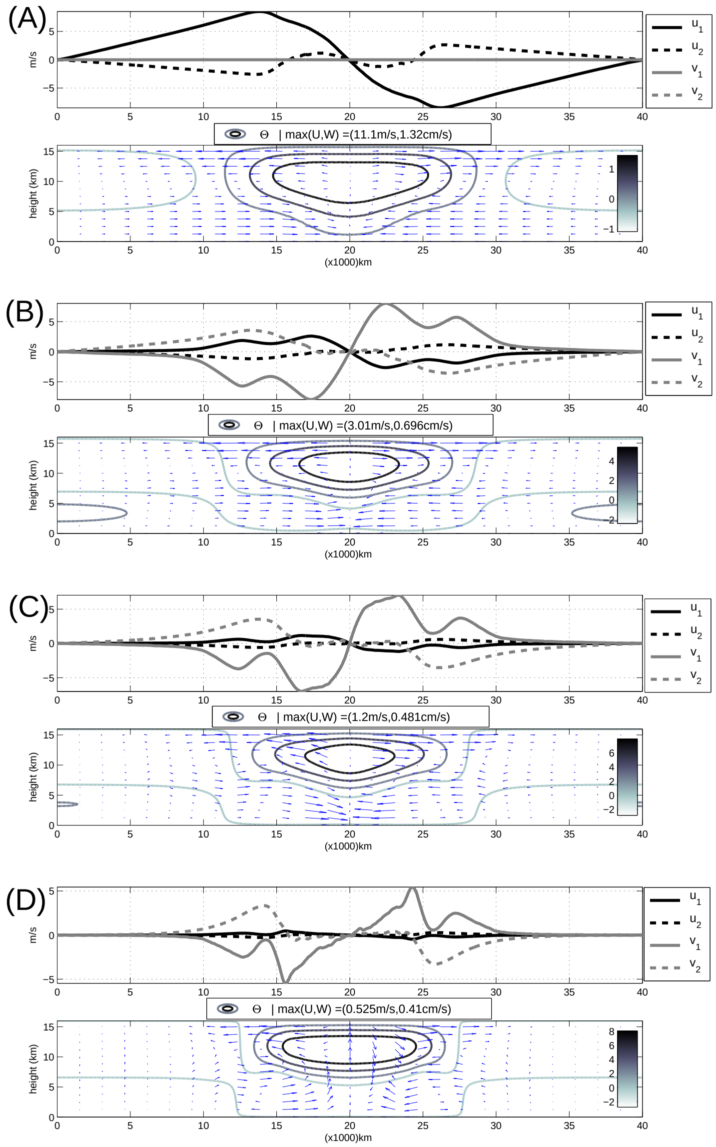

Fig. 11 Same as Fig. 10 but for $\bar{\theta}_{eb} - \bar{\theta}_{em} = 14$ K.

498 ## 5 Concluding discussion

499 Convection in the tropics is organized into a hierarchy of mesoscale clusters
500 and superclusters with scales ranging from the convective cell of a few kilo-

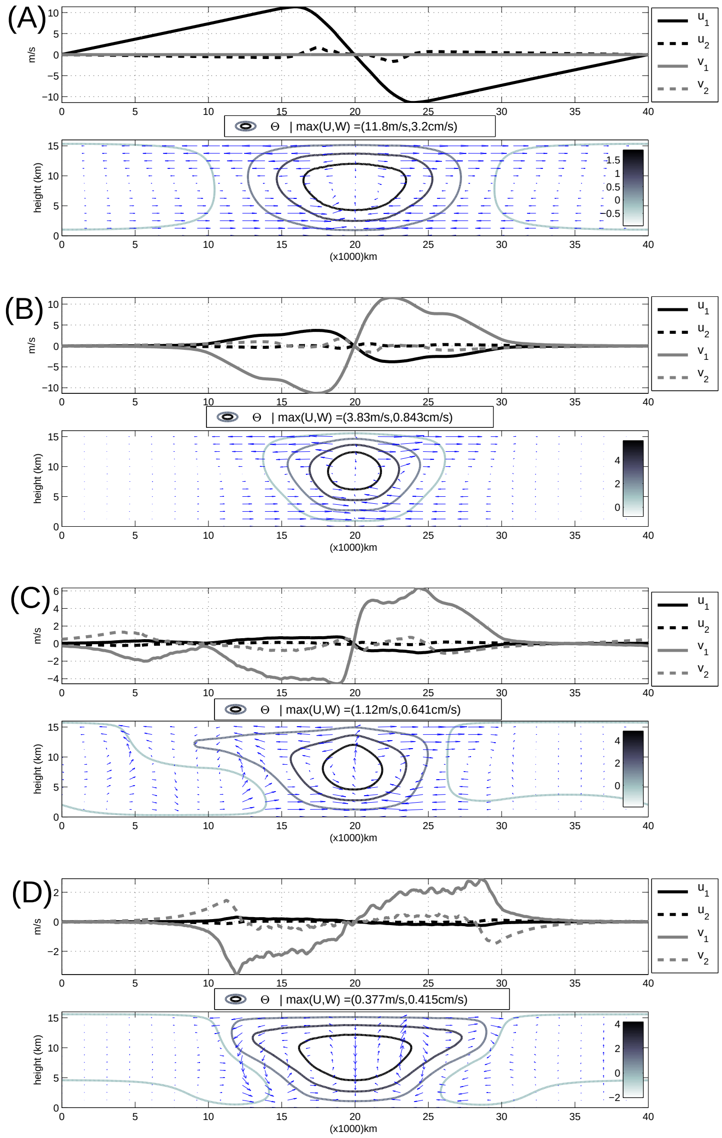

Fig. 12 Same as Fig. 10 but for $\bar{\theta}_{eb} - \bar{\theta}_{em} = 20$ K.

meters to planetary scale disturbances. As a consequence of the tremendous effort devoted by the scientific community, significant progress has been made during the last few decades in our understanding of the dynamics and physical features of the associated multiscale waves such as meso-scale convective sys-

Table 8 Standard deviation (u_1 m/s, u_2 m/s, q K) for the warm pool SMCM simulations using the FMK13 regime.

Latitude	$\theta_{eb} - \theta_{em} = 10$ K	$\theta_{eb} - \theta_{em} = 14$ K	$\theta_{eb} - \theta_{em} = 20$ K
0^o	30.5, 47.6, 162	25.4 ,62.1 ,75.1	62.4, 85.2, 118.5
5^o	2.5, 11.0, 6.75	2.5, 10.5 ,6.5	3.5,12.5, 7.5
10^o	1.5,5.0 , 3.3	1.0 ,6.0 ,3.1	1.5,5.2 ,5.3
20^o	0.5,4.0 , 1.5	0.5 ,5.0 ,1.8	1.0,4.5 ,3.3

tems, convectively coupled tropical waves and the MJO [33, 21, 27, 19]. While mesoscale convective systems are found almost all over the world especially near the coasts and mountains, curiously, synoptic and planetary scale convectively coupled waves are restricted to the tropics and to some extent to the subtropics. The main physical properties that distinguish the tropics from the midlatitudes are the abundance of mid-tropospheric moisture and the vanishing of the Coriolis force at the equator. To shed some light into this outstanding conundrum we used simple deterministic and stochastic multicloud models to study the effect of rotation and mid-tropospheric dryness on organized convection and convectively coupled gravity waves. The effect of rotation on convection has been studied previously by Liu and Moncrieff using cloud resolving modeling [22] on a $4,000$ km synoptic scale domain. We have chosen to use the multicloud model, because it captures well the observed dynamical and physical features of organized convection and convectively coupled waves, including the MJO [15, 18, 17, 20, 13, 2, 3] and allows for simple linear stability analysis.

Linear analysis for two-dimensional flows parallel to the equator is performed in Section 3 in two typical parameter regimes of the deterministic multicloud model, the KM08 [18] and the FMK13 [2] regimes. In the KM08 regime, the main effect of rotation and mid-tropospheric moisture on convectively coupled gravity waves is that their growth rates decrease significantly as the Coriolis force is increased and/or the mid-tropospheric moistness is decreased. Instead the system gives rise to an instability of a standing-congestus mode whose growth rates increase with the mid-tropospheric dryness and the band of unstable modes increases with both the rotation and mid-tropospheric dryness. The FMK13 regime on the other hand does not produce a standing congestus mode but the growth rates of the moist gravity waves consistently decrease with increased rotation and with increased mid-tropospheric dryness. We note that the main differences between the two parameter regimes are in, γ_2', the relative contribution of θ_2 to congestus heating and the deep convective inverse buoyancy time scale parameter, a_0. Both assume larger values in the KM08 regime but γ_2' is substantially larger. The fading of the moist gravity wave instability in the dry atmosphere and for higher Coriolis parameter values is consistent with the fact that convectively coupled waves are found mostly in the tropics. We assessed whether any one of these unstable modes obeys the weak temperature gradient (WTG) balance [31] by comparing the relative contribution of each term in the the θ equations. We found that while the first baroclinic mode component of the moist gravity wave can be considered in WTG balance, the second baroclinic cannot. Thus, transient dynamics associated with the second baroclinic mode can be an obstacle for using straightforward WTG theories [31] to parametrize tropical convection. However, more sophisticated multi-scale WTG approximation that allow for gravity waves on larger scales have already proved useful for analyzing many multi-scale features of tropical convection [24, 25, 19].

The role of the congestus mode is apparent in the nonlinear deterministic simulations performed in the KM08 regime with homogeneous and warm pool SST backgrounds. In the homogeneous SST in particular, the congestus mode forces the emergence of a Walker-type steady zonal mean flow. Such steady circulation was reported in [18] but it is further amplified when the Coriolis force is introduced and increased. More importantly, as the Coriolis force or dryness is increased the wave fluctuations associated with the MGWI decrease progressively in intensity and the whole solution becomes ultimately evanescent; the meridional component of the mean circulation increases with rotation and dominates the mean circulation. Note also that the wavelength of the steady-mean flow decreases with increasing f consistent with the increase of the instability band of the congestus instability toward small scales. The decay of moist gravity wave fluctuations is also observed when a warm pool forcing is imposed. However, the key feature here resides in the induced Walker circulation which becomes shallower and shallower and more confined to the vicinity of the warm pool, while the mean meridional circulation increases and dominates as f increases. The shallow circulation observed at higher latitudes is consistent with the dominance of the congestus mode which is associated with the second baroclinic mode reminiscent of the persistence of congestus cloud decks on the flanks of the ITCZ [11].

Another contribution of this article comes from the use of the stochastic multicloud model (SMCM) to address this question about the effect of rotation and mid-tropospheric dryness on convection. As pointed out in [2,3], the SMCM captures very well the chaotic behavior and stochastic organization of tropical convection as observed in cloud resolving modeling and in nature [30]. As shown in Section 4.3, the multiscale organization of convection into streaks of synoptic scale patterns associated with moist gravity waves and their planetary scale envelopes, fades out when the Coriolis parameter is increased from 5^o to 20^o. As the Coriolis parameter is increased convection becomes very patchy and unorganized and strikingly similar to that seen in CRM simulations of Liu and Moncrieff [22] which are performed under similar conditions on a smaller domain. The same behavior is observed for both the small dryness values of $\bar{\theta}_{eb} - \bar{\theta}_{em} = 11$ K and for the moderate one of $\bar{\theta}_{eb} - \bar{\theta}_{em} = 14$ K, although the transition is more rapid in the latter case.

Acknowledgement This research of AJM is partially supported by ONG grant N00014-11-1-0306 which supports YF as a postdoctoral fellow as well as the Center for Prototype Climate Modeling at NYU Abu Dhabi. The research of BK is partly supported by the Natural Sciences and Engineering Research Council of Canada.

References

1. Dias, J., Pauluis, O.: Impacts of Convective Lifetime on Moist Geostrophic Adjustment. Journal of Atmospheric Sciences **67**, 2960–2971 (2010). DOI 10.1175/2010JAS3405.1
2. Frenkel, Y., Majda, A.J., Khouider, B.: Using the stochastic multicloud model to improve tropical convective parameterization: A paradigm example. J. Atmos. Sci. **69**, 1080–1105 (2012)
3. Frenkel, Y., Majda, A.J., Khouider, B.: Stochastic and deterministic multicloud parameterizations for tropical convection. Climate Dynamics (2013). DOI 10.1007/s00382-013-1678-z
4. Frierson, D., Majda, A., Pauluis, O.: Dynamics of precipitation fronts in the tropical atmosphere. Comm. Math. Sciences **2**, 591–626 (2004)
5. Gadgill, S.: The indian monsoon and its variability. Annu. Rev. Earth Planet. Sci. **31**, 429–467 (2003)
6. Goswami, B.N., Mohan, R.S.A., Xavier, P.K., Sengupta, D.: Clustering of low pressure systems during the indian summer monsoon by intraseasonal oscillations. Geophys. Res. Lett. **30**, 8 (2003). DOI doi: 10.1029/2002GL016,734
7. Gu, G., Zhang, C.: Cloud components of the ITCZ. J. Geophy. Res. **107**, (D21) 4665 (2002). DOI doi:10.1029/2002JD002089
8. Gu, G., Zhang, C.: A spectral analysis of westward-propagating synoptic-scale disturbances in the ITCZ. J. Atmos. Sci. **59**, 2725–2739 (2002)
9. Gu, G., Zhang, C.: Westward-propagating synoptic-scale disturbances and the ITCZ. J. Atmos. Sci. **59**, 1062–1075 (2002)
10. Han, Y., Khouider, B.: Convectively coupled waves in a sheared environment. J. Atmos. Sci. **67**, 2913–2942 (2010)
11. Johnson, R.H., Rickenbach, T.M., Rutledge, S.A., Ciesielski, P.E., Schubert, W.H.: Trimodal characteristics of tropical convection. Journal of Climate **12**(8), 2397–2418 (1999)

12. Khouider, B.: A coarse grained stochastic particle interacting system for tropical convection. Comm. Math. Sci. p. (Submited) (2013)
13. Khouider, B., Biello, J., Majda, A.J.: A stochastic multicloud model for tropical convection. Comm. Math. Sci. **8**(1), 187–216 (2010)
14. Khouider, B., Han, Y., Majda, A., Stechmann, S.: Multi-scale waves in an MJO background and CMT feedback. J. Atmos. Sci. **69**, 915–933 (2012)
15. Khouider, B., Majda, A.J.: A simple multicloud parametrization for convectively coupled tropical waves. Part I: Linear analysis. J. Atmos. Sci. **63**, 1308–1323 (2006)
16. Khouider, B., Majda, A.J.: A simple multicloud parametrization for convectively coupled tropical waves. Part II: Nonlinear simulations. J. Atmos. Sci. **64**, 381–400 (2007)
17. Khouider, B., Majda, A.J.: Equatorial convectively coupled waves in a simple multicloud model. J. Atmos. Sci. **65**, 3376–3397 (2008)
18. Khouider, B., Majda, A.J.: Multicloud models for organized tropical convection: Enhanced congestus heating. J. Atmos. Sci. **65**, 897–914 (2008)
19. Khouider, B., Majda, A.J., Stechmann, S.N.: Climate science in the tropics: waves, vortices and pdes. Nonlinearity **26**(1), R1 (2013). URL http://stacks.iop.org/0951-7715/26/i=1/a=R1
20. Khouider, B., St-Cyr, A., Majda, A.J., Tribbia, J.: The MJO and convectively coupled waves in a coarse-resolution GCM with a simple multicloud parameterization. J. Atmos. Sci. **68**(2), 240–264 (2011)
21. Kiladis, G.N., Wheeler, M.C., Haertel, P.T., Straub, K.H., Roundy, P.E.: Convectively coupled equatorial waves. Rev. Geophys. **47**, RG2003, doi:10.1029/2008RG000,266 (2009)
22. Liu, C., Moncrieff, M.W.: Effects of Convectively Generated Gravity Waves and Rotation on the Organization of Convection. Journal of Atmospheric Sciences **61**, 2218–2227 (2004)
23. Liu, C., Moncrieff, M.W.: Explicit Simulations of the Intertropical Convergence Zone. Journal of Atmospheric Sciences **61**, 458–473 (2004). DOI 10.1175/1520-0469(2004)061
24. Majda, A.J.: New multi-scale models and self-similarity in tropical convection. J. Atmos. Sci. **64**, 1393–1404 (2007)
25. Majda, A.J., Rupert, K.: Systematic multiscale models for the tropics. J. Atmos. Sci. **60**, 393–408 (2003)
26. Majda, A.J., Stechmann, S.N., Khouider, B.: Madden-julian oscillation analog and intraseasonal variability in a multicloud model above the equator. Proc. Nat. Acad. Sci. **104**, 9919–9924 (2007)

27. Moncrieff, M.W., Waliser, D.E., Caughey, J.: Progress and direction in tropical convection research: YOTC International Science Symposium. Bulletin of the American Meteorological Society **93**, 65 (2012). DOI 10.1175/BAMS-D-11-00253.1

28. Mounier, F., Janicot, S.: Evidence of two independent modes of convection at intraseasonal timescale in the West African summer monsoon. Geophys. Res. Lett. **31**, L16116 (2004). DOI 10.1029/2004GL020665

29. Nie, J., Boos, W.R., Kuang, Z.: Observational evaluation of a convective quasi-equilibrium view of monsoons. J. Climate **23**, 4416–4428 (2010)

30. Peters, K., Jakob, C., Davies, L., Khouider, B., Majda, A.: Stochastic behaviour of tropical convection in 1 observations and a multicloud model. J. Atmos. Sci. p. accepted (2013). DOI 10.1175/JAS-D-13-031.1

31. Sobel, A.H., Nilsson, J., Polvani, L.M.: The weak temperature gradient approximation and balanced tropical moisture waves. J. Atmos. Sci. **58**(23), 3650–3665 (2001)

32. Straub, K.H., Kiladis, G.N.: Interactions between the Boreal Summer Intraseasonal Oscillation and Higher-Frequency Tropical Wave Activity. Monthly Weather Review **131**, 945 (2003)

33. Zhang, C.: Madden–Julian Oscillation. Reviews of Geophysics **43**, G2003+ (2005). DOI 10.1029/2004RG000158